Journal of Magnetism and Magnetic Materials 332 (2013) 21–27

Contents lists available at SciVerse ScienceDirect

Journal of Magnetism and Magnetic Materials

journal homepage: www.elsevier.com/locate/jmmm

Complex magnetic interactions and charge transfer effects in highly ordered Ni_xFe_{1-x} nano-wires

Shu-Jui Chang, Chao-Yao Yang, Hao-Chung Ma, Yuan-Chieh Tseng*

Department of Materials Science & Engineering, National Chiao Tung University, 1001 Ta Hsueh Road, Hsin-Chu 30010, Taiwan, ROC

ARTICLE INFO

Article history:
Received 23 October 2012
Received in revised form
12 November 2012
Available online 3 December 2012

Keywords:
NiFe
Nano-wires
XMCD
Charge transfer

ABSTRACT

This work investigates the subtle magnetic interactions within the Ni_xFe_{1-x} ($x=0.3$, 0.5, and 1.0) nano-wires by probing spin-dependent behaviors of the two constituted elements. The wires were fabricated by electro-deposition and an anode aluminum oxide template to produce free-standing nature, and the Ni–Fe interactions were probed by x-ray magnetic spectroscopy across a BCC→FCC structural transition. The wires' magneto-structural properties were predominated by Ni, as reflected by a decrease but an increase in total magnetization and FCC x-ray intensity with increasing x, even if the Fe moment increased simultaneously. Upon annealing, a prominent charge transfer, together with the changes of spin-dependent states, took place in the Ni and Fe 3d orbitals, and a structural disordering was also obtained, for the wires at $x=0.3$. The charge transfer led to a local magnetic-compensation for the two elements, explaining the minor change in total magnetization for $x=0.3$ probed by a vibrational sample magnetometer. When x was increased to 0.5, however, the charge transfer became inactive due to persistent structural stability supported by Ni, albeit resulting in nearly invariant magnetization similar to that of $x=0.3$. The complexity of the Ni–Fe interactions varied with the composition and involved the modifications of the coupled magnetic, electronic and structural degrees of freedom. The study identifies the roles of Ni and Fe as unequally-influential in Ni_xFe_{1-x}, which provides opportunities to re-investigate the compound's properties concerning its technological applications.

1. Introduction

Because permalloy ($Ni_{80}Fe_{20}$) [1,2] and invar ($Ni_{65}Fe_{35}$) [3,4] alloys are the central components of many modern technologies, shaping Ni_xFe_{1-x} into various forms in a controllable manner, and investigating the varying properties corresponding to the shaping have captured great research popularity. Although the properties of Ni_xFe_{1-x} have been reported in several systems [5,6], probing Ni–Fe interactions in nanostructures continues to provide a playground for realizing the compound's fundamental properties, as well as for developing principles to create the functional structures.

Motivated by this cause, we combined pulse-electrodeposition and an anodic aluminum oxide (AAO) template to fabricate Ni_xFe_{1-x} nano-wires with a precise control over the size and shape. The wires' coupled magnetic, electronic and structural degrees of freedom that determine the wires' macroscopic magnetism were realized by the element-specific probes of Ni and Fe. An annealing-induced, spin-dependent Ni–Fe charge transfer effect was especially focused in this study. The modifications in microscopic magnetism, and associated electronic re-establishments, are often neglected if changes in macroscopic magnetism are imperceptible. Nevertheless, the invisible electronic interactions are essential, as they drive the magnetic ordering, also serving as the cause for many anomalous effects. This is a serious concern in Ni_xFe_{1-x}, because the compound disobeyed the Slater–Pauling prediction [7,8] at certain compositions, depending on the system and treatment [9,10]. This implies that the magnetism of Ni_xFe_{1-x} is not simply the sum of the local moments of Ni and Fe but rather depends on the local interactions of the two. The interactions may vary with x, because increasing x altered the crystallographic structure of Ni_xFe_{1-x} [5,6]. The underlying physics is still under debate due to incomplete understanding of Ni_xFe_{1-x} and hence is worthy of exploration.

Using x-ray magnetic spectroscopy, we successfully discriminated the magnetisms of Ni and Fe with varying x. Further, employing rapid thermal annealing (RTA) we were able to create structural instability, and examine the correlation between the structural instability and the wires' magnetic and electronic responses with x-dependency, based on the isolated Ni(Fe) behaviors. We discovered a flow of spins from Fe to Ni 3d conduction band when the structural stability was lost, despite

* Corresponding author. Tel.: +886 35731898; fax: +886 35724727.
E-mail address: yctseng21@mail.nctu.edu.tw (Y.-C. Tseng).

0304-8853/$ - see front matter © 2012 Elsevier B.V. All rights reserved.
http://dx.doi.org/10.1016/j.jmmm.2012.11.037

the total magnetization of the wires remaining almost unaltered. This resulted in a decrease but an increase in Fe and Ni local moments, together with the changes of the electronic states of the two. The element-specific probe uncovered the local magnetic-compensation of the wires invisible to the conventional probes, perfectly explaining the minor change in magnetization upon annealing. However, such phenomenon was absent when the structural stability was persistent, which can be related to the increased dominance of Ni. In summary this work investigates the properties of the Ni_xFe_{1-x} bimetallic wires from a microscopic picture. This work subverts our thoughts that the two elements are equally-influential in Ni_xFe_{1-x}, and therefore opens research opportunities concerning the compound's properties from both technical and fundamental aspects.

2. Experimental

Pulse-electrodeposition method combined with an AAO template were used to fabricate highly aligned Ni_xFe_{1-x} nano-wires with varying compositions ($x=0.3$, 0.5, and 1). To do so, a commercial AAO featuring 60 μm in thickness and 0.25 μm in pore-diameter (aspect-ratio=300) was patterned by a Ti/Cu electrode only on one side using a sputtering facility, where Ti served as an adhesion layer between the AAO and the Cu seed layer. The AAO inter-pore distance was about 0.45 μm. The Cu seed layer of the Ti/Cu electrode was not completely homogeneous, so an extra Cu-electrodeposition on the AAO/Ti/Cu was followed to provide better quality of Cu, operating at a deposition current of 15 mA and a deposition time of 1.5 h. Afterwards, the AAO/Ti/Cu was immersed into a deposition bath containing $FeSO_4 \cdot 7H_2O$, $NiSO_4 \cdot 6H_2O$, H_3BO_3 and ascorbic acid, subjected to an electrodeposition operated at 30 mA and a total duration of 20 min. The deposition was pulse-based, with an interval of 1 s between current-on and -off, at which on and off were both held for 1 s in an alternating manner for the entire deposition. Since the pulse-delay time (T_{off}) was kept constant, the anomalous co-deposition of Ni and Fe that may result in a higher deposition rate of Fe, as suggested by Salem et al. [11], was not expected in our case. The concentrations of Ni and Fe were controlled by the use of $FeSO_4 \cdot 7H_2O$ and $NiSO_4 \cdot 6H_2O$, and were identified by energy dispersive spectrometry (EDX), subsequent to the removal of the wires from the substrate. The EDX analysis only showed Ni and Fe signals, which excluded the possibility that Cu electrode may form the alloy with NiFe upon annealing. RTA of 300 °C-2 min was applied to the samples, and the annealed samples were compared with the non-annealed ones in terms of all analyses. The samples' morphologies, crystallographic structures and magnetic properties were identified using a scanning electron microscope (SEM), an x-ray diffraction (XRD) facility and a vibrating sample magneto-meter (VSM), respectively, all without the AAO protection. The wires' magnetic easy-axis was found to be the long-axis, so the magnetic hysteresis (M–H) curves presented here were all taken from the long-axis measurements. A high-resolution transmission electron microscope (HRTEM, JEM-2100F, operated at 200 keV) was used to probe the microstructure of the wires. To further understand the wires' magnetism with elemental specificity, x-ray absorption spectroscopy (XAS) and x-ray magnetic circular dichrosim (XMCD) taken with total electron yield (TEY) and total fluorescence yield (TFY) modes were employed to probe the spin-dependent states of Ni and Fe, at BL11A, National Synchrotron Radiation Research Center (NSRRC). The XMCD spectra were taken by having the x-ray photon wave-vector parallel to the wires' long-axis under an applied field of 1 T. This forced the Ni and Fe moments to be measured in a way parallel to the wires' easy-axis, which promised a quantitative comparison with the VSM data. Each XAS/XMCD spectrum presented in this work was the average of more than 5 data points collected on different spots of the same sample, and the deviation was very minor among the spectra, which suggests the sample homogeneity to be of reliable quality. Finally, spin (S_z) and orbital (L_z) moments were estimated by sum-rule analysis [12] to elucidate the Ni and Fe moments in a detailed way. The use of n_{3d} in sum-rule analysis was carefully treated, as detailed in the text, considering the varying electronic states of Ni and Fe.

3. Results and discussion

Fig. 1(a) shows the SEM image of the Ni_xFe_{1-x} nano-wires on the Ti/Cu electrode after the AAO removal, where the high-ordering, free-standing nature of the wires can be clearly assessed. The wires' dimensions were precisely controlled by the AAO and they were identical for all compositions in order to have a quantitative comparison in magnetic properties. Upon the RTA, the morphologies of the wires remain unaltered as confirmed by Fig. 1(b). The isolations of the wires were well preserved as demonstrated by SEM with a larger magnification.

We first focus on the wires without the RTA treatment. Fig. 2(a) shows the x-dependent M–H curves for the wires. The saturation field and coercive field of the wires highly depend on the manufacturing recipe [13–15], aspect-ratio [16] and pore-diameter [11,14,17,18]. In our case, the saturation field is larger than 5000 Oe and the coercive field is about 75 Oe in average.

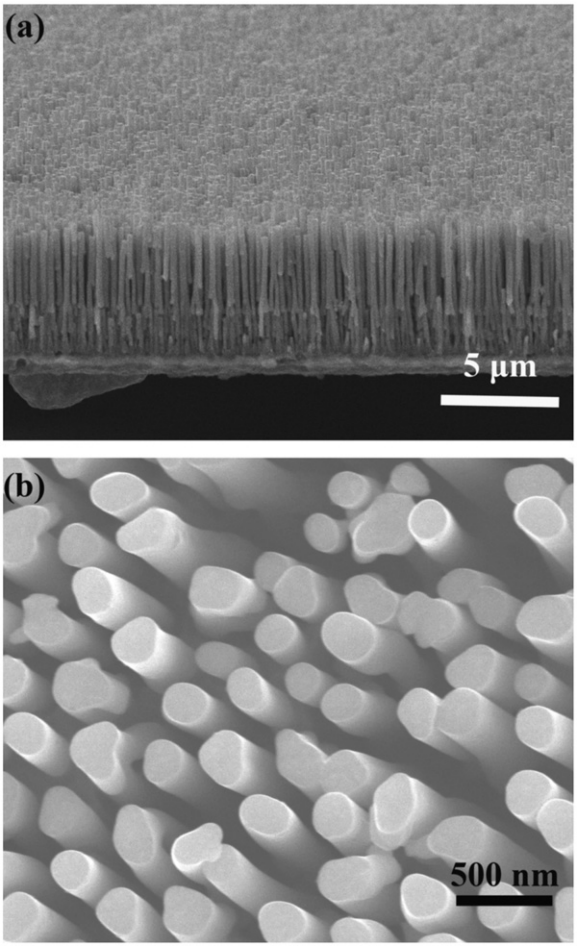

Fig. 1. (a) Cross-sectional SEM image of the as-deposited Ni_xFe_{1-x} nano-wires and (b) top-viewed SEM image of the annealed Ni_xFe_{1-x} nano-wires, with a larger magnification.

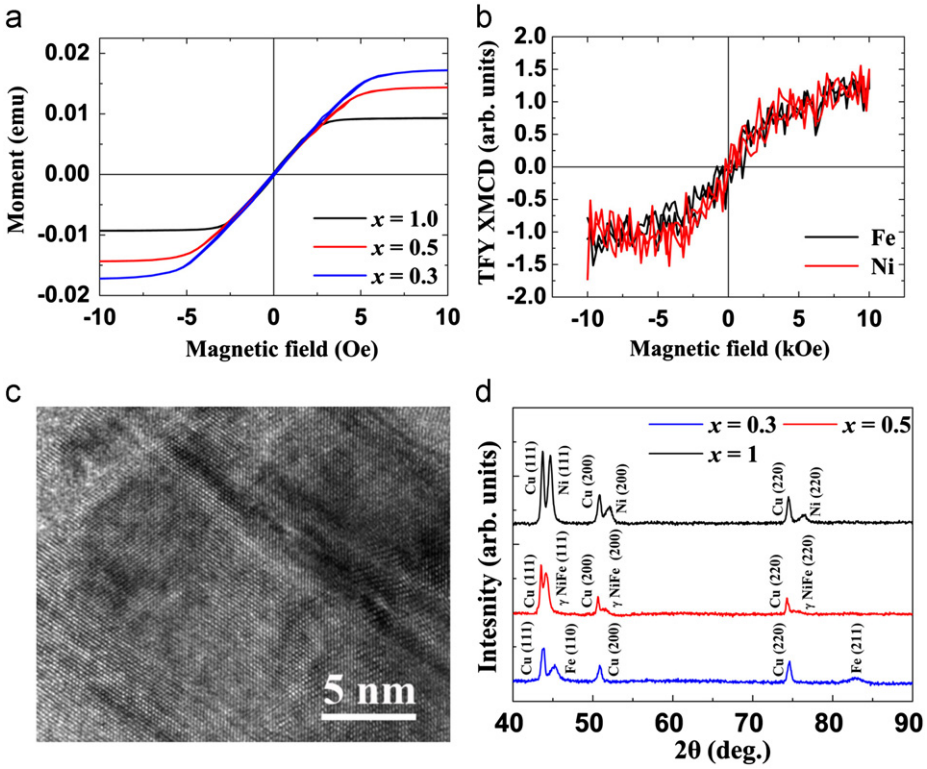

Fig. 2. (a) x-Dependent M–H curves. (b) TFY M–H curves of Fe (black) and Ni (red) for $x=0.5$, and the same curve is seen in $x=0.3$. (c) HRTEM image of $x=0.5$. Similar polycrystalline microstructure is seen in $x=1.0$ and 0.3. (d) x-dependent XRD patterns. For the FCC–BCC mixed phase case as $x=0.5$, the characteristic peaks are hard to identify so they are not indexed. However, for $x=0.3$, the characteristic peaks are close to Fe BCC so they are indexed. (For interpretation of the references to color in this figure legend, the reader is referred to the web version of this article.)

The wires appear to lose saturation magnetization (M_s) with increasing x. This suggests that the role of Ni is to reduce the wire's magnetization, agreeing well with the general picture of the Slater–Pauling curve [9,10]. Element-specific M–H curves performed over the L_3-edges of Ni and Fe are given in Fig. 2(b). The Ni and Fe share similar field-dependency as shown in the M–H curves probed by the VSM (Fig. 2(a)), suggesting that the two elements are coherent in magnetization reversal. A HRTEM image demonstrating a homogeneous polycrystalline microstructure for $x=0.5$ is shown in Fig. 2(c). Similar micrograph is seen in other samples (hence, not provided), in agreement with the literatures [9,18] reporting that the electro-deposition generally produces a polycrystalline microstructure for nano-materials.

Upon the introduction of Ni, a structural transition takes place, changing from mainly BCC ($x=0.3$) [19], then BCC+FCC ($x=0.5$) [5,17,20] and finally to FCC ($x=1.0$) [21], as shown in Fig. 2(d). The structural transition can be tracked by the transition of the characteristic peaks; i.e., the Fe BCC-(110) setting at 45.23 degree ($x=0.3$), then shifting to a lower angle of 44.15 degree corresponding to the BCC–FCC mixed case ($x=0.5$), and finally relocating at a higher angle of 44.76 degree assigned by Ni FCC-(111) ($x=1.0$). The transition of the characteristic peaks is consistent with Glaubitz et al. [5] also dealing with a BCC→FCC transition in the Ni_xFe_{1-x} thin films. It came to our attention that the structural ordering of the Fe-rich sample is weaker than that of the Ni-rich sample, from the fact that the Fe-rich sample's ($x=0.3$) XRD intensity is less pronounced than that of the Ni ($x=1.0$) one. One may notice that the intensity of Cu (111) increases with increasing x, therefore arguing that the crystallization of Ni could have been facilitated by a better crystallized Cu electrode, rather than an intrinsic property of Ni itself. However, all the AAO/Ti/Cu substrates were prepared in the same batch and the quality-variation was very minor. This can be validated by the comparable peak intensities of Cu (200) and Cu (220) from sample to sample. Therefore, the enhanced intensity of Cu (111) could be explained as having an overlap with the Ni (111) but not the quality-variation of the electrode. Thus, the results imply that the Ni FCC is more energetically favored within the wire structure. This could explain the dominance of Ni over the wire's magnetic properties as detailed below, considering that the structural and magnetic properties are often coupled in magnetic materials [22–25].

The Ni and Fe XAS spectra with varying x are presented in Fig. 3(a) and (b), respectively. Both Ni and Fe are found to be oxidized by the evidence of edge-splitting. In general, Fe is more sensitive to oxidation than Ni due to a higher oxidation potential [26], and the oxidation that can be easily acquired at the L_3 as this edge, especially with the TEY XAS, is renowned for fingerprinting the chemical state of Fe [27–30]. In XAS, x-dependency is almost imperceptible for Ni and Fe. However, XMCD reflecting the Ni and Fe moments exhibits opposite dependencies with x. In Fig. 4(a), the Ni XMCD intensity is found to decrease with increasing x. Conversely, the Fe XMCD intensity not only increases but also turns to be more metallic-like with increasing x, as presented in Fig. 4(b). For $x=0.5$ in particular, its Fe XMCD line-shape deviates from those of Fe_2O_3 and Fe_3O_4 [27,28] but is rather similar to metallic Fe [5,12], which suggests that the oxidation is minor for this concentration. Also, from the TEM results (not shown) we did not obtain any oxidized layer at the wire's surface. For Fe, the XAS with light oxidation but the XMCD with a metallic spectral shape can be found in Tsai et al. [29] and Kim et al. [30], for the cases of CoFeB/MgO thin films and Fe substrate, respectively, very similar to our situation. In both references Fe was treated to be metallic and ferromagnetic considering the limited oxidation effect, and therefore the same principle can be followed for $x=0.5$ here. However, the Fe oxidation cannot be neglected in $x=0.3$, as the oxidation effect is evident in the XMCD spectral shape.

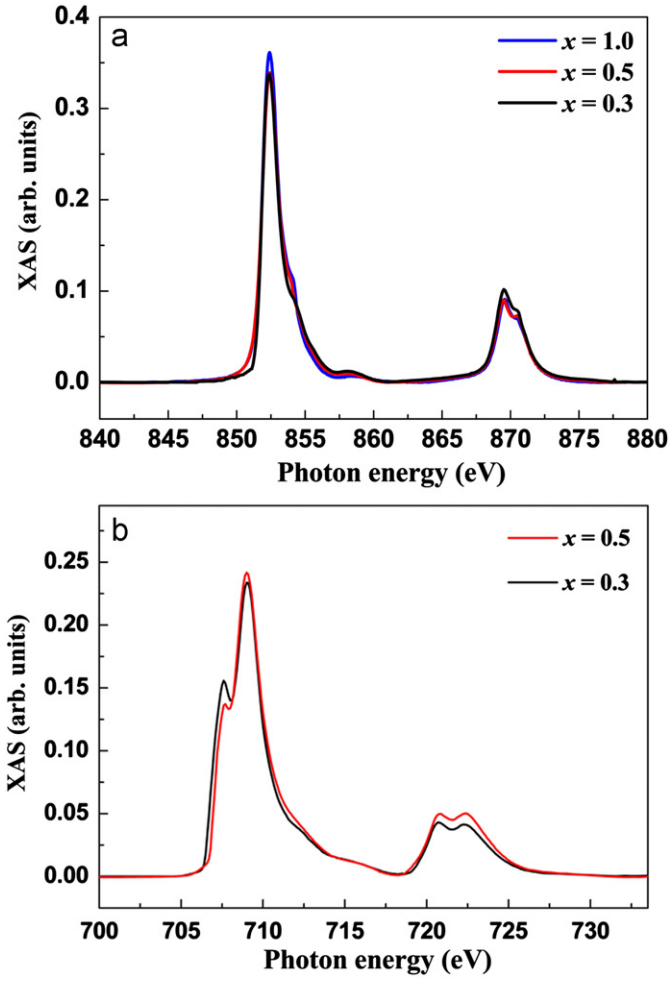

Fig. 3. x-Dependent (a) Ni L_2, L_3 XAS and (b) Fe L_2, L_3 XAS.

Fig. 4(c) presents the x-dependent sum-rule analyses (S_z+L_z) for Ni and Fe. Qualitatively, the microscopic analyses from the sum rule are consistent with the macroscopic analyses from the VSM throughout the paper, indicating the reliability of the analyses. The sum-rule results suggest that Ni and Fe exhibit contrary dependencies, where the Fe moment increases, whereas the Ni moment decreases, with increasing x. The increased Fe moment can be explained by the more metallic and enhanced Fe XMCD as x increases from 0.3 to 0.5 (Fig. 4(b)), while the decreased Ni moment can be understood as the suppressed XMCD signal, with increasing x, after spectral normalization [31]. The weighted sum of Ni and Fe presumably equals to the total magnetization of Ni_xFe_{1-x}, which decays with increasing x. It is noteworthy that the same trend has been discovered in Fig. 8 of Glaubitz et al. [5]. Both Glaubitz's and our results show the fact that despite Ni_xFe_{1-x} following the Slater–Pauling prediction for magnetism, Ni and Fe take contrary paths locally, in spite of their coherent magnetization reversal. Interestingly, despite unclear mechanism for the decreased Ni moment with increasing x, when concentration is weighted Ni's magnetic strength is still sufficient to pull down the wire's total magnetization matching the Slater–Pauling prediction. In combination with the XRD (Fig. 2(c)), Ni seems to be more dominant than Fe in terms of magnetic and structural degrees of freedom, as will be further validated by the results from the RTA in the following.

Now we turn focus to the RTA effects particularly for $x=0.3$ and 0.5 samples. Fig. 5(a) and (b) presents the M–H curves and XRD patterns for $x=0.3$ affected by the RTA, respectively. The saturation magnetization drops by only 5% with the RTA, so the magnetism is affected by the treatment in a very minor way. However, for $x=0.3$, notable changes are obtained in the Ni/Fe XAS (Fig. 5(c) and (d)), with the Ni and Fe XAS white-line intensities being suppressed and enhanced, respectively. The XAS here corresponds to the Ni/Fe 2p→3d photo-excitation process with the white-line intensity reflecting the available vacancy in the 3d orbital. Since Ni exhibits suppressed intensity than that of Fe, it indicates a charge transfer from Fe to Ni via orbital hybridization that results in higher d-band vacancy of Fe, i.e., a more oxidized state for Fe but a more reduced state for Ni, under the influence of the RTA. The more oxidized state for Fe is due to a more pronounced intensity in L_3 pre-edge, while a more reduced state for Ni is linked to the suppressed XAS along with the disappearance of the shoulders around the edges.

The charge transfer consequently modifies the spin-polarizations of the two constituents as reflected by their XMCD, as given in Fig. 5(e) and (f). For Ni, the suppressed XAS gives rise to an enhanced XMCD as a consequence. Conversely, oscillation emerges in the Fe XMCD around the L_3, indicating a highly oxidized Fe as Fe_2O_3 and Fe_3O_4 [27,28]. In Fig. 5(b), the Fe BCC is found to disappear after the RTA. In fact, a heavily smeared peak near Cu (111) is barely detectable in the XRD of the annealed $x=0.3$, which can be due to the disappeared Fe (110). This indicates that some degrees of structural ordering still persist upon RTA to support the magnetic hysteresis observed in Fig. 5(a), but it is difficult to be identified due to limited resolution of the x-ray facility, so we rather prefer to claim the phase to be close to amorphous. This is unusual because the heat treatment usually facilitates the crystallization of the materials especially in bulk forms. However, since the Ni_xFe_{1-x} is formed in nano-wires, the large thermal stress raised by the RTA in a very short period is unlikely to be relieved within such a low and confined dimension, and therefore causes deterioration of the structure, especially when the structural ordering is intrinsically weak prior to the RTA. Here, the Ni–Fe charge transfer occurs with the disappearance of Fe (110), perhaps due to more overlapped Ni/Fe 3d electron wave-functions with the structural disordering, and examples of structural-disordering induced charge transfer can be referred to from Refs. [32–34]. Since the magnetic and structural properties are strongly coupled, the annealing-induced structural disordering would modify the magnetism of Ni_xFe_{1-x} accordingly. Interestingly, though the modification is obscure with a macroscopic probe, it is unambiguously probed by a microscopic one, hence revealing the importance of the latter.

Fig. 6 presents the sum-rule results (S_z+L_z) for Ni and Fe before and after the RTA, for $x=0.3$. Considering the substantial changes in the chemical states of Ni and Fe, n_{3d} for both metallic and fully oxidized (Ni^{2+}, Fe^{3+}) cases were used in various combinations to examine if any deviation in the trend of (S_z+L_z) is seen. The deviation was less than 15% for the extreme case and had no significant influence on the trend. The results reveal that the charge transfer is spin-dependent, resulting in a decrease but an increase in the Fe and Ni moments. Therefore, the minor magnetization change probed by the VSM (Fig. 5(a)) can be understood as a local magnetic-compensation. It arises from the spin exchange between the two elements with the loss of structural stability, a phenomenon invisible to the conventional measurement.

For $x=0.5$, the magnetization also drops imperceptibly after the RTA, as shown in Fig. 7(a). However, the induced structural disordering is less pronounced than that of $x=0.3$, as the characteristic peaks of the mixed-phase are still visible in Fig. 7(b), especially the peak near Cu(111). The persistence of structural stability deactivates the electronic modifications of Ni and Fe, as reflected by their XAS provided in Fig. 7(c) and (d), respectively.

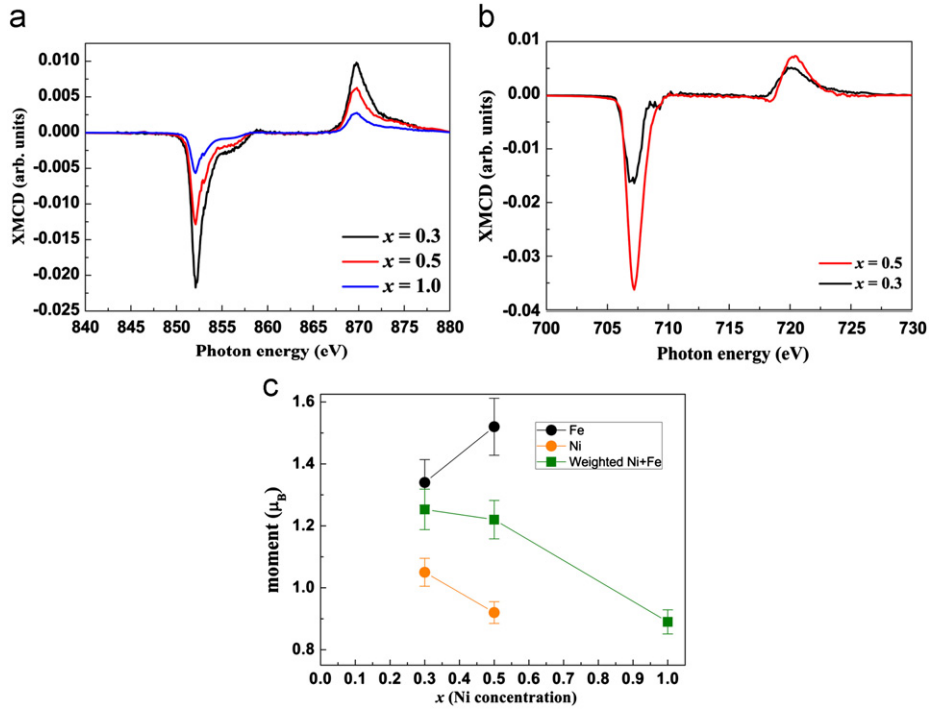

Fig. 4. *x*-Dependent (a) Ni L_2, L_3 XMCD and (b) Fe L_2, L_3 XMCD. All spectra are normalized to the integrations of corresponding XAS spectra. (c) Sum-rule (S_z+L_z) analyses for Ni, Fe, and weighted Ni+Fe, with *x*-dependency. In (c), lines through data points are guides for the eyes, and the scale of the *y*-axis is selectively presented for the purpose of clarity.

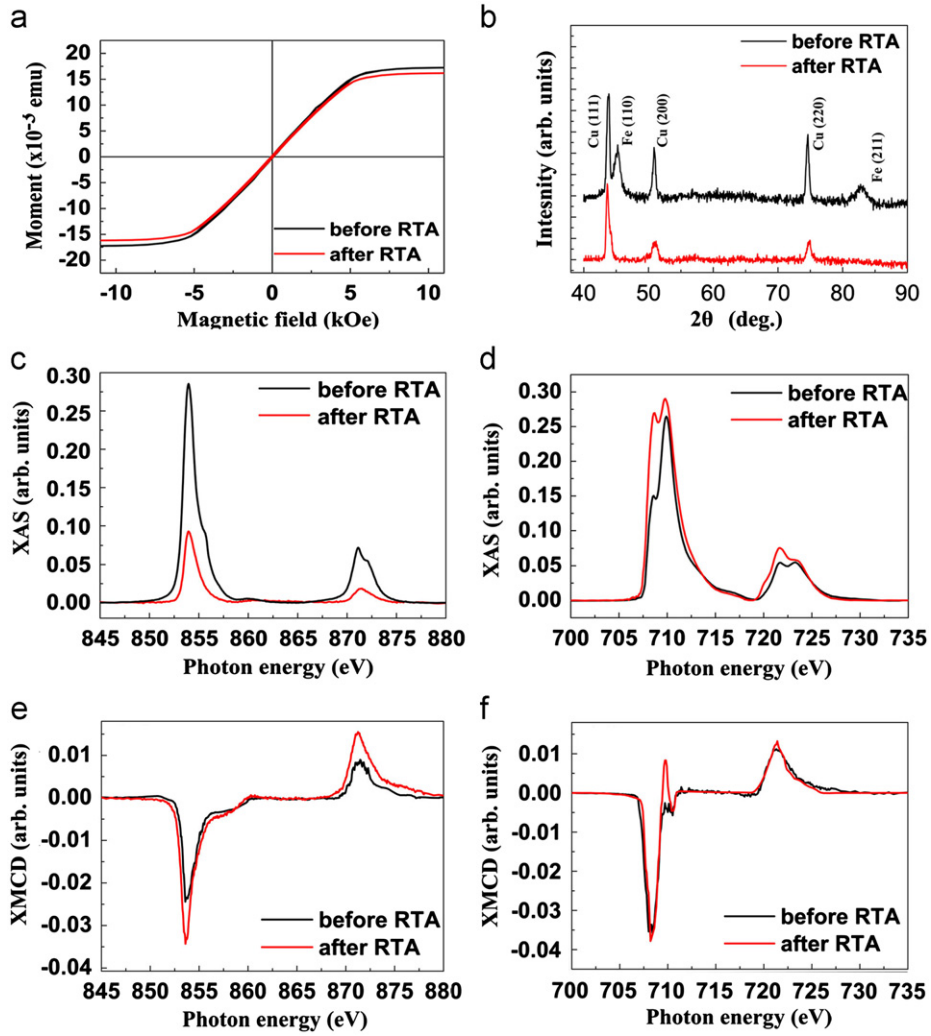

Fig. 5. (a) *M*–*H* curves (b) XRD patterns (c) Ni L_2, L_3 XAS (d) Fe L_2, L_3 XAS (e) Ni L_2, L_3 XMCD and (f) Fe L_2, L_3 XMCD, for $x=0.3$ before and after the RTA treatment.

Here, the Ni XAS remains unaltered, but a minor deviation is obtained in the Fe XAS after the RTA, and a likeness is seen in their XMCD (Fig. 7(e) and (f)). The identical Ni XAS before and after the RTA suggests no electronic-modification; i.e., no charge transfer in the Ni conduction band. Thus, the limited change in the Fe XAS can be realized as the minor oxidation at the surface, instead of the electron removal as that happened at $x=0.3$. Apparently, the charge transfer effect is both composition- and structure-dependent. It only occurs when the structural stability is lost such as $x=0.3$. However, for $x=0.5$, the charge transfer is invisible, due to the robust structural stability supported by the larger fraction of the Ni FCC. The results indicate that the properties of Ni_xFe_{1-x} are complex, involving the interactions among the magnetic, structural and electronic degrees of freedom which all vary with x, and are probably hard to be predicted by the Slater–Pauling curve alone. In particular, the role of Ni is found to be supreme in Ni_xFe_{1-x} as it dominates the total magnetization and structural stability, and thus its influence should be more weighted than Fe, which is essential for attempts to tailor the properties of Ni_xFe_{1-x}.

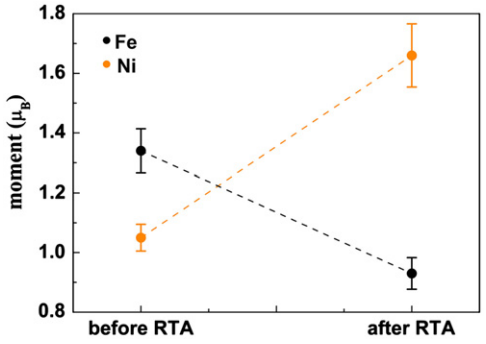

Fig. 6. Sum-rule (S_z+L_z) analyses for Ni, Fe, for $x=0.3$ before and after the RTA treatment. The scale of the y-axis is selectively presented for the purpose of clarity.

In bimetallic magnetic compounds, we find that if one of the constituents dominates the magnetic properties, there must be at least a physical parameter, such as crystal or electronic structure itinerantly coupled with the magnetism of the dominant constituent, to support its dominance. For example, in Yang et al. [23] only 6% of Co doping was sufficient to alter the magnetic phase of the Ni rod along with the change of microstructure from nanocrystalline to polycrystalline. In Telling et al. [35], Co was more magnetically dominant than Mn in Co_2MnAl, due to a smaller gap in the Co minority spin-band. Even in the theoretical work Wang et al. [36] pointed out that in a Cu–Co bimetallic cluster system,

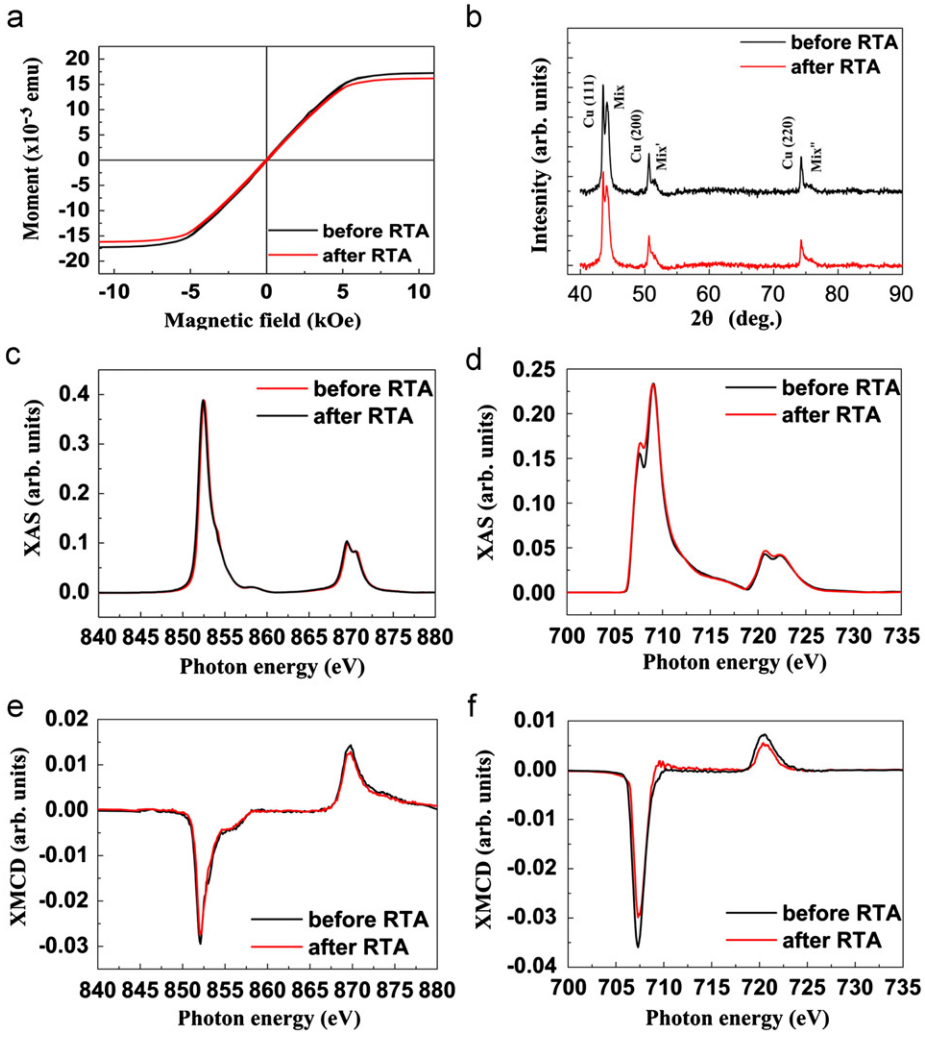

Fig. 7. (a) M–H curves (b) XRD patterns (c) Ni L_2, L_3 XAS (d) Fe L_2, L_3 XAS (e) Ni L_2, L_3 XMCD and (f) Fe L_2, L_3 XMCD, for $x=0.5$ before and after the RTA treatment. In (b), Mix, Mix′ and Mix″ represent the three characteristic peaks of the BCC–FCC mixed phase just near the characteristic peaks of Cu, and these peaks are still observable after the RTA.

the introduction of Cu atoms would cause a dramatic enhancement of magnetism due to geometrical characters. All these phenomena suggest that, in a bimetallic system the physical proximity effects would lose balance if any two physical degrees of freedom of one constituent are more coupled than the other constituent. This will lead to the dominance of the constituent with the stronger coupling, if one of its degrees of freedom is elaborated. Assigning this principle to our case, we elaborate the structural instability to imbalance the physical proximity effect between Ni and Fe, which sharply discriminates the electronic responses of the two. Correlating the structural information with the local and macroscopic magnetism, it is easy to observe the dominance of Ni in Ni_xFe_{1-x}. Finally, the invariant magnetizations with the RTA for $x=0.3$ and 0.5, therefore, need to be described by different microscopic pictures. For the former, it results from the spin exchange between Ni and Fe. However, the latter is characterized by the static, inactive interactions between the two elements as a result of the persistent structural stability.

4. Conclusion

In this study we have demonstrated how Ni–Fe magnetic interactions influenced the Ni_xFe_{1-x} nano-wires' magneto-structural properties, by isolating the Ni and Fe elemental behaviors while the wires underwent the structural transition. The influences of the two elements were found to be incomparable, with Ni being superior to Fe in terms of magnetic and structural properties. Upon RTA, the wires at $x=0.3$ became amorphous, where the Ni and Fe moments compensated mutually by exchanging the 3d electrons. This reasoned the nearly unaltered magnetization of the wires. A similar macroscopic behavior was seen at $x=0.5$, while its invariant magnetization needed to be described as the inactive electronic interaction between the two elements, because of persistent structural properties resulting from a larger fraction of Ni.

Acknowledgment

The authors appreciate the assistances on HRTEM, XMCD, and electro-deposition from Dr. C.M. Liu, Dr. H.J. Lin and Mr. K.M. Chen, respectively. This work is supported by the National Science Council of Taiwan, under Grant no. NSC 98-2112-M-009 022-MY3.

References

[1] M. Kläui, Journal of Physics: Condensed Matter 20 (2008) 313001.
[2] C.L. Dennis, R.P. Borges, L.D. Buda, U. Ebels, J.F. Gregg, M. Hehn, E. Jouguelet, K. Ounadjela, I. Petej, I.L. Prejbeanu, M.J. Thornton, Journal of Physics: Condensed Matter 14 (2002) R1175–262.
[3] O. Yamada, E.T. Lacheisserie, Journal of the Physical Society of Japan 53 (1984) 729–734.
[4] E.F. Wassermann, Journal of Magnetism and Magnetic Materials 100 (1991) 346.
[5] B. Glaubitz, S. Buschhorn, F. Brussing, R. Abrudan, H. Zabel, Journal of Physics: Condensed Matter 23 (2011) 254210.
[6] B. Singh, C.L. Ho, Y.C. Tseng, C.T. Lo, Journal of Nanoparticle Research 14 (2012) 706.
[7] J. Crangle, G.C. Hallam, Proceedings of the Royal Society A 272 (1963) 119.
[8] R.F. Willis, N.J. Gilman, Europhysics Letters 69 (2005) 411.
[9] K.H. Lee, H.Y. Lee, W.Y. Jeung, W.Y. Lee, Journal of Applied Physics 91 (2002) 8513.
[10] A. Cai, H. Zhang, H. Hua, Z. Zhang, Nanotechnology 13 (2002) 627.
[11] M.S. Salem, P. Sergelius, R. Zierold, J.M. Montero Moreno, D. Görlitz, K. ielsch, Journal of Materials Chemistry 22 (2012) 8549.
[12] C.T. Chen, Y.U. Idzerda, H.J. Lin, N.V. Smith, G. Meigs, E. Chaban, G.H. Ho, E. Pellegrin, F. Sette, Physical Review Letters 75 (1995) 152.
[13] F.E. Atalay, H. Kaya, Journal of Alloys and Compounds 469 (2009) 458.
[14] S. Aravamudhan, J. Singleton, Journal of Physics D: Applied Physics 42 (2009) 115008.
[15] C.G. Wu, H.L. Lin, Journal of Solid State Electrochemistry 10 (2006) 198.
[16] H.R. Khan, K. Petrikowski, Journal of Magnetism and Magnetic Materials 213 (2000) 526.
[17] Q. Liu, J. Wang, Z. Yan, D. Xue, Physical Review B 72 (2005) 144412.
[18] F. Tain, J. Zhu, D. Wei, Journal of Physical Chemistry C 111 (2007) 12699.
[19] J.B. Wang, X.Z. Zhou, Nanotechnology 15 (2004) 485.
[20] Y.B. Zhu, Y. Wang, X.Y. Zhang, G.W. Qin, International Journal of Refractory Metals and Hard Materials 25 (2007) 275.
[21] X.W. Wang, G.T. Fei, Journal of Physical Chemistry B 109 (2005) 24326.
[22] C.C. Huang, C.C. Lo, Y.C. Tseng, C.M. Liu, C. Chen, Journal of Applied Physics 109 (2011) 113905.
[23] C.Y. Yang, C.C. Huang, Y.C. Tseng, C.M. Liu, C. Chen, Journal of Applied Physics 110 (2011) 073913.
[24] C. Magen, L. Morellon, P.A. Algarabel, M.R. Ibarra, C. Ritter, A.O. Pecharsky, K.A. Gschneidner Jr., V.K. Pecharsky, Physical Review B 70 (2004) 224429.
[25] D. Haskel, Y.B. Lee, B.N. Harmon, Z. Islam, J.C. Lang, G. Srajer, Ya. Mudryk, K.A. Gschneidner Jr., V.K. Pecharsky, Physical Review Letters 98 (2007) 247205.
[26] 〈http://www.siliconfareast.com/ox_potential.htm〉.
[27] E. Pellegrin, M. Hagelstein, S. Doyle, H.O. Moser, J. Fuchs, D. Vollath, S. Schuppler, M.A. James, S.S. Saxena, L. Niesen, O. Rogojanu, G.A. Sawatzky, C. Ferrero, M. Borowski, O. Tjernberg, N.B. Brookes, Physica Status Solidi (b) 215 (1999) 797.
[28] L. Signorini, L. Pasquini, F. Boscherini, E. Bonetti, I. Letard, S. Brice-Profeta, P. Saincavit, Nuclear Instruments and Methods in Physics Research Section B 246 (2006) 20.
[29] W.C. Tsai, S.C. Liao, H.C. Hou, C.T. Yen, Y.H. Wang, H.M. Tsai, F.H. Chang, H.J. Lin, C.H. Lai, Applied Physics Letters 100 (2012) 172414.
[30] D.H. Kim, H.J. Lee, G. Kim, Y.S. Koo, J.H. Jung, H.J. Shin, J.-Y. Kim, J.-S. Kang, Physical Review B 79 (2009) 033402.
[31] All XMCD spectra presented in this work were normalized to the integrations of corresponding XAS spectra, which was to guarantee the comparison based on an atomic absorption.
[32] N.R. Khasanova, F. Izumi, M. Shida, B.C. Chakoumakos, E. Ohshima, M. Kikuchi, Syono, Physica C 269 (1996) 115.
[33] S.A. Bewick, R.A. Pascal, D.M. Ho, Z.G. Soos, M. Masino, Journal of Chemical Physics 122 (2005) 024710.
[34] M. Zhang, M.R. Anderson, Langmuir 10 (1994) 2807.
[35] N.D. Telling, P.S. Keatley, G. van der Laan, R.J. Hicken, E. Arenholz, Y. Sakuraba, M. Oogane, Y. Ando, K. Takanashi, A. Sakuma, T. Miyazaki, Physical Review B 78 (2008) 184438.
[36] J. Wang, G. Wang, X. Chen, W. Lu, J. Zhao, Physical Review B 66 (2002) 014419.